FEA Report

Hamish McNeill

April 2026

Abstract

A running prosthetic is assessed with Aluminium 2014 T4 and CFRP as materials, and iterated upon according to the resonance, fatigue and weight of the product, with the assistance of various FEA methods. The modified design is more durable and less prone to resonance while running, although it may lack in its ability to spring the user forward.

Contents

1 Introduction **2**
- 1.1 Background . . . 2
- 1.2 Objectives . . . 2
- 1.3 Preliminary 2D Tests . . . 2
- 1.4 Modified Design . . . 4

2 Methods **4**
- 2.1 Boundary Conditions . . . 4
- 2.2 Mesh . . . 4
- 2.3 Fatigue . . . 6
- 2.4 Resonance . . . 7

3 Results **8**
- 3.1 Mesh Refinements . . . 8
- 3.2 Initial Design . . . 9
- 3.3 Modified Design . . . 10

4 Discussion **10**
- 4.1 Failure . . . 10
- 4.2 Radii . . . 12
- 4.3 Resonance . . . 12
- 4.4 Comparison . . . 13

5 Conclusion **13**

A Derivation of N and Q **14**

B Stress Heat Maps **15**

C Life Heat Maps **17**

1 Introduction

1.1 Background

When running with a prosthetic, the blade is exposed to regular shocks from the ground that are carried into the leg. It is important that the blade does not resonate with the running motion or the frequencies of the shock waves from ground collisions. It is also important that the blade lasts a long time without being too heavy to perform athletically.

For the benefit of runners who make use of a prosthetic leg, it is therefore worthwhile to develop a benchmark for running-specific prosthetic leg designs against the metrics of material fatigue and resonance.

1.2 Objectives

The objective of this report is to assess the fatigue and vibrational properties of a running-specific prosthetic leg made of both Aluminium 2014 T4 and Carbon fibre reinforced composite (CFRP), and then propose an improved design for those metrics, while ensuring that weight is not unreasonably increased.

Design Specification:	
Resonant modes	>50Hz
Lightweight	
Lifespan under fatigue	≥1,000,000 cycles

Table 1: Design specifications of improved running-specific prosthetic (RSP).

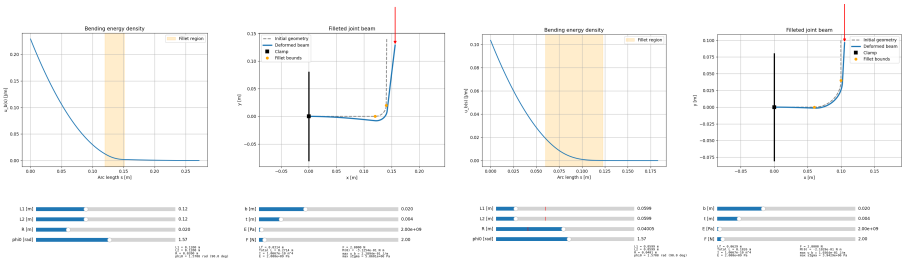
The RSP design used is taken from Mitu (2014) [5] as its schematics are publicly available. Studies have already been done on the FEA of this design [1], although not for its fatigue behaviour.

The proposed design changes were based on hypotheses that were validated using a stand-alone python program using SciPy for FEA in 2D, written by the author with the assistance of GitHub Copilot [2] for frontend code that used tkinter. Some simulations were also made in python with SciPy to use beam theory without FE.

1.3 Preliminary 2D Tests

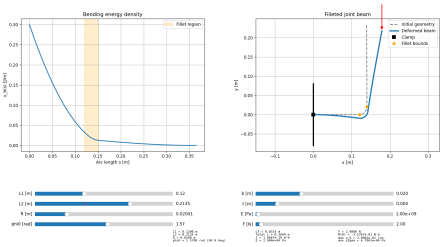
In order to inform the modified design iteration, several simulated tests were conducted.

Firstly, using beam theory, a filleted right-angle bend was modelled with a shear point force at one extremity and a fixed support at the other, and it was

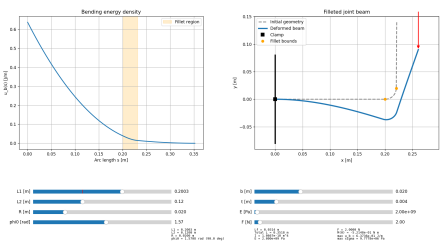


(a) Original.

(b) Increased radius.



(c) Increased trail-off.



(d) Increased leverage.

Figure 1: Simulation of filleted right-angled beam under planar elastica treatment.

shown in Figure 1 that a wider radius (1b) would lower the maximum stress and increase the effective stiffness. It was also shown that decreasing either the straight segment L1 (1d) or L2 (1c) would have a contrary effect.

For the next test, the FEA program with a 2D beam editor and FE treatment with C0 interpolation was used. Cascading arcs of differing radii were simulated next to a single arc (Figure 2), and by lowering the average curvature, the maximum stress was reduced.

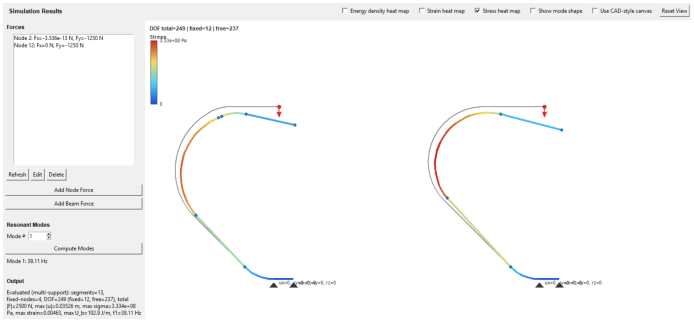


Figure 2: Comparison of cascading arcs to single arc fillet.

1.4 Modified Design

If we model with beam segments, then we find that the only degrees of freedom of the design are straight segment lengths and fillet radii, followed by cross-sectional width and height, which can also be optimised. Due to the fixed load and the total dimensions of the design, the performance metric of the work done on the material $\mathrm{d}W = \frac{1}{2}\sigma\varepsilon\mathrm{d}V$ is also a performance metric of the number of straight segments required, hence the modified design consisted of greater fillet radii and a modest increase in the number of segments to accommodate it.

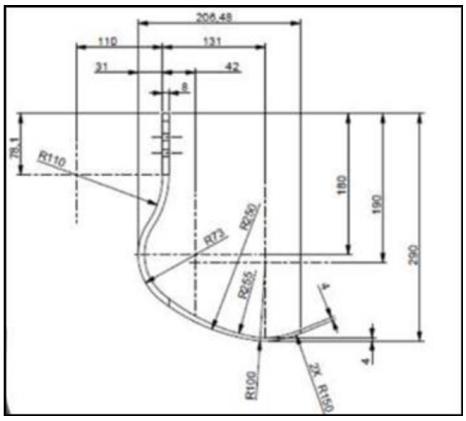


Figure 3: 2D Schematic of original design [1].

2 Methods

2.1 Boundary Conditions

The weight of an average man (70kg) [7] is multiplied by an engineering factor of 3 to form a 2100N. The paper from which the design originates uses a 1500N load, an engineering factor of 2.

When the blade hits the ground, the bottom of the blade is dragged against the ground in the opposite direction to the motion of the runner. Therefore friction force was modelled in the direction of travel of the runner. Using a reasonable estimate of the coefficient of friction [3], we arrive at approximately 500N of friction force.

Since the blade is back-mounted, the top end is mechanically fastened vertically to the back of the prosthetic leg, forming a fixed support that prevents translation and rotation of this fastened section.

2.2 Mesh

The correct mesh must balance the number of parameters with computational resources in order to reasonably minimise the error in the predictions of the

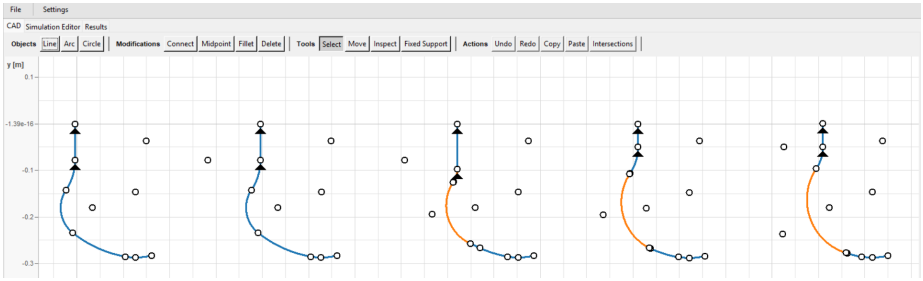


Figure 4: Sketches.

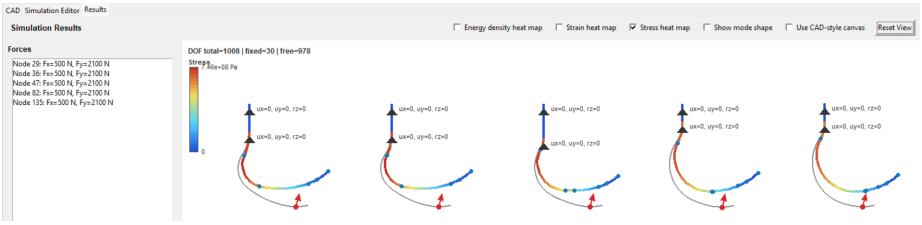


Figure 5: 2D Beam element FEA.

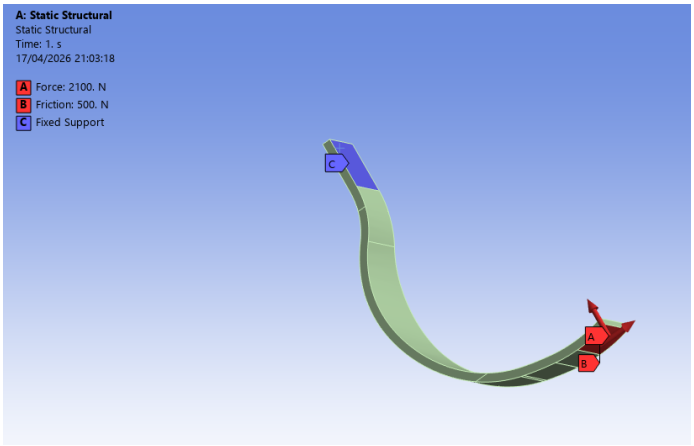


Figure 6: Screenshot of forces and supports applied to original design model.

model.

Assuming the element size error is the root mean square error (RMSE) of the correct resonance mode/fatigue life, a local minimum of error exists where the derivative of RMSE with respect to element size is negative and approaches 0.

The derivative of RMSE is $\pm 2f\frac{\mathrm{d}f}{\mathrm{d}r}$ where f is the resonance frequency and r is element size. We assume the negative because we assume error reduces with

element size. Element size was reduced until accuracy returns diminished to 1% or computational resources were exceeded.

Golden Section Search was used to find this value, since the RMSE with respect to element size is a unimodal function, and we lack information about its derivatives.

Soft behaviour was selected for local resizing with only 2 layers of elements, since the design is not particularly intricate and the elements are smaller in scale than the design's features.

2.3 Fatigue

The use-case for the RSP will be of rapid cycles of compression as the user presses the blade into the ground with each step, before releasing for each other step. There will also be a negligible period of slight tension when the blade is in the air and begins to accelerate downward again; load cycles were modelled with a stress ratio of zero.

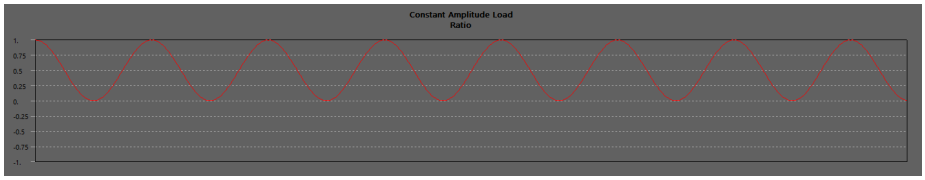


Figure 7: Load cycle setting.

Since aluminium is a ductile material, it was not appropriate to model the mean stress correction with the Goodman curve. Instead, the Gerber curve was used to account for the mean, non-cyclical component of stress.

According to the study cited in Figure 8, CFRP is a brittle material. Therefore, the Goodman curve was used to correct the mean stress for the analysis with CFRP.

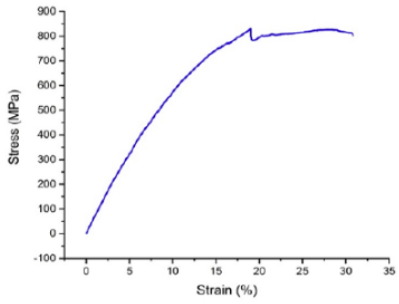
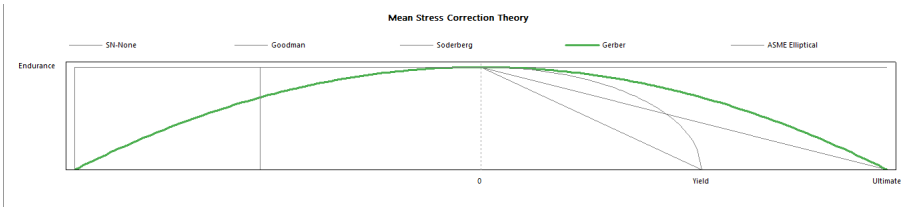


Figure 6. Stress–strain curve of CFRP composite

Figure 8: Stress-strain curve of CFRP [6].



(a) Gerber fatigue graph.



(b) Goodman fatigue graph.

Figure 9: Graphs for selected mean stress correction functions.

Von Mises equivalent stress was selected as the stress measurement for fatigue analysis for the Aluminium test because von Mises equivalent stress is shown to be more empirically reliable for ductile materials, due to their higher sensitivity to shear stress. For brittle materials, maximum principal stress is more reliable, hence it was used for the simulations with CFRP.

Before evaluating material life, S-N data was required for both materials. The S-N data for aluminium 2014 T4 was already included in the Ansys Mechanical 2025R2 engineering database, however for CFRP data was found from experimental data cited in Figure 10.

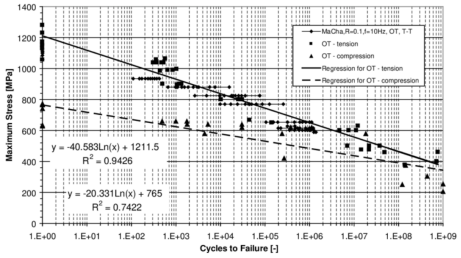


Figure 10: Empirical data for CFRP S-N curve [4].

2.4 Resonance

Since the target for the lowest resonant frequency is 50Hz, much processor time can be conserved by limiting the search range to 0-500Hz, as we are not interested in higher resonant modes.

The direct solver was selected for higher accuracy since the modal analysis required relatively less computational capacity.

3 Results

Heat maps for stress and life are presented in Appendices B and C respectively, due to being too numerous.

3.1 Mesh Refinements

For our purposes, mesh refinement via GSS entails reducing the element size by a factor of the Golden Ratio until convergence of computational capacity is reached.

Despite seeing a large spike in maximum stress at 1.80mm, at 1.11mm, processor resources were exceeded for hexahedral elements and values were not retrieved; therefore, a global element size of 1.80mm was selected.

High Jacobian ratios were seen for the 1.80mm and 1.11mm mesh sizes indicating that the mesh adhered to the assumption of a Jacobian ratio of 1, as well as reasonable aspect ratios measured as a sanity check.

Size /mm	Elements	Aspect Ratio Avg. ± Std.	Jacobian Ratio Avg. ± Std.	Max. Stress /GPa	% Change	Frequency /Hz	% Change
20.0	81	2.65±0.494	0.859±0.0873	0.95107		96.008	
12.4	215	1.73±0.305	0.902±0.0709	0.94767	-0.36	95.992	-1.7
7.64	469	2.89±2.13	0.877±0.105	0.98943	4.4	96.41	0.44
4.72	1298	2.73±1.34	0.916±0.0417	0.94093	-4.9	95.855	-0.58
2.92	6444	2.11±1.12	0.961±0.0266	0.92012	-2.2	96.002	0.15
1.80	23540	1.57±0.428	0.985±0.00826	1.0412	13	96.542	0.56
1.11	99774	2.17±1.42	0.986±0.0165	NA		NA	

Table 2: Change in initial model behaviour as mesh element size decreases.

3.2 Initial Design

The schematics for the initial design (Figure 3) were adapted into a 3D CAD drawing for FEA.

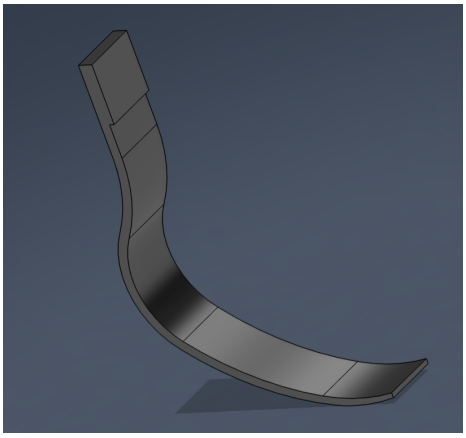


Figure 11: Image of initial RSP 3D CAD model.

Material	Mass /kg	Frequency /Hz	Max. Stress	Cycles
Aluminium 2014 T4	0.483	80.865	0.4678	0
Carbon Fibre (CFRP)	0.293	96.542	1.0412	0

Table 3: Performance indices of the initial design made of Aluminium 2014 T4 vs. CFRP.

3.3 Modified Design

After experimenting with radii and segment lengths using the python FEA software, an enlargement was added around the high-stress fillet region, followed by a chamfered support strut at the upper bend to lower the strain concentrations at those areas.

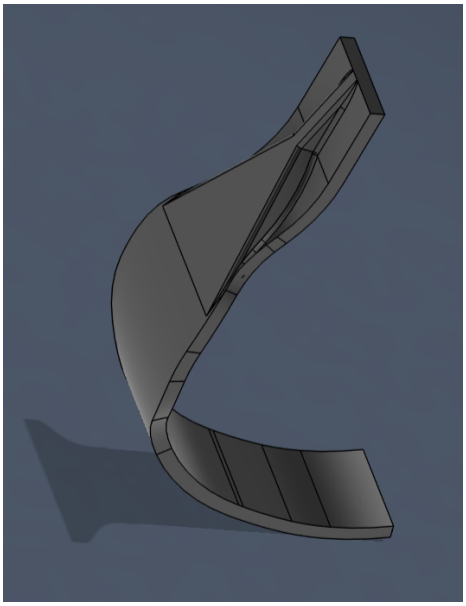


Figure 12: Image of modified RSP design.

The final design mesh was constructed of 322308 quadratic tetrahedral elements (tet10), and had an average Jacobian ratio (Gauss) of 0.99885 with a standard deviation of 0.0108.

Material	Mass /kg	Frequency /Hz	Max. Stress	Cycles
Aluminium 2014 T4	0.594	109.67	0.34805	18112
Carbon Fibre (CFRP)	0.361	139.08	0.68043	916

Table 4: Performance indices of the modified design made of Aluminium 2014 T4 vs. CFRP.

4 Discussion

4.1 Failure

Material failure occurs when the activation energy at a certain point is reached to break the chemical bonds at that point. Therefore, work done on a finite

element by a load determines after how many cycles that finite element tears. Therefore the material failure will happen at the point of maximum energy density, which relates to the von Mises criterion as follows.

Deviatoric strain energy density $u_{ij}^{dev} = \int \sigma \mathrm{d}\varepsilon$ evaluates to $\frac{1}{2}E\varepsilon_{ij}^2$, which can be expressed as $\frac{s_{ij}\varepsilon_{ij}}{2}$. Since deviatoric strain $\varepsilon_{ij} = \frac{s_{ij}}{2G}$ in tensor form where G is the shear modulus, we have

$$u^{dev} = \sum_{i,j} u_{ij}^{dev} = \frac{1}{4G}\sum_{i,j} s_{ij}^2 : s_{ij} = \sigma_{ij} - \frac{1}{3}\mathrm{tr}(\sigma)\delta_{ij}$$

where $\frac{1}{3}\mathrm{tr}(\sigma)$ is the average normal pressure and δ_{ij} is the Kronecker delta. If this work were done by an equivalent uniaxial (von Mises) stress σ_v, then the principal stresses would be $\sigma_1 = \sigma_v, \sigma_2 = \sigma_3 = 0$, so

$$s_{11} = \sigma_v - \frac{1}{3}\sigma_v = \frac{2}{3}\sigma_v,\ s_{22} = s_{33} = 0 - \frac{1}{3}\sigma_v = \frac{-1}{3}\sigma_v$$

and

$$u^{dev} = \frac{1}{4G}(\frac{4}{9}\sigma_v^2 + \frac{1}{9}\sigma_v^2 + \frac{1}{9}\sigma_v^2) = \frac{\sigma_v^2}{6G}$$

Therefore, the critical activation energy for ductile material failure u_{crit}^{dev} corresponds directly to a critical deviatoric yield stress S_y expressed as an equivalent von Mises stress σ_v.

Volumetric strain energy density $u_k^{uni} = \int \sigma \mathrm{d}\varepsilon$ similarly can be expressed in terms of principal stress as

$$u^{uni} = \frac{1}{6K}\sum_k \sigma_k^2$$

where K is the bulk modulus. Brittle volumetric yield stress S_u depends only on principal stress, and so we must express the stress tensor only in terms of these by diagonalising it.

$$\Sigma = S\begin{bmatrix}\sigma_1 & 0 & 0\\ 0 & \sigma_2 & 0\\ 0 & 0 & \sigma_3\end{bmatrix}S^T$$

Since stress tensors are real and symmetric, the orthogonal matrix S is always a rotation matrix, so we are simply rotating each finite element in the brittle material to observe all stress and strain energy as volumetric.

As expected, the points of failure in both designs were also the points of highest stress since these were the locations with highest strain energy.

The drop in maximum stress in the modified design compared to the original design can be explained by the increases in the cross-sectional area normal to the load F. The stress peaked at the lower ends of the wings because the corners act as stress raisers, but stress was also lower in regions of greater cross-sectional area. These peak stresses would have been greater if the corners were not rounded. This is demonstrated by the peak stress in the sharp corner of the initial design.

4.2 Radii

From Appendix A, there is an established relation between force $N(s) = \sigma(s)A$ and curvature θ'

$$N'' + q_t' + \theta'^2 N + \theta' q_n = 0$$

given the assumption of small deflections, where q_t and q_n are tangential and normal internal distributed loads. This equation describes the resultant normal pressure, with a $\theta'^2 N$ term analogous to the Coriolis effect. From this it is clear that a decrease in curvature θ' would lower the contribution to the pressure of the normal force for each node and lower the effective pressure throughout the fillet. This effect was already validated in the preliminary 2D tests and is necessary for the lower stress seen in the fillets of the modified design.

4.3 Resonance

In a 1D driven elastic system that obeys $mx'' + kx = \sin \alpha t$, a resonance occurs when $\alpha = \omega$, such that $\omega^2 = \frac{k}{m}$, which can be shown if complementary functions sin and cos are assumed. Therefore, it is intuitive that increasing stiffness k is worthwhile.

Resonant modes of frequency of an oscillating system can be found if the system is elastic such that $M\mathbf{R}'' + K\mathbf{R} = 0$, as the eigenvalues ω^2 of KM^{-1}.

$$(K - \omega^2 M)\mathbf{R} = 0 \Rightarrow |KM^{-1} - \omega^2 I| = 0$$

Using the Raleigh quotient and strain energy U formula:

$$\omega^2 = \frac{\mathbf{v}^T K \mathbf{v}}{\mathbf{v}^T M \mathbf{v}},\ U = \frac{1}{2}\mathbf{v}^T K \mathbf{v}$$

where v is a vector of displacements and U is the strain energy given these displacements, we find that increasing the required strain energy for a deformation increases the frequency of the resonant mode. This is expected as the energy of oscillation must increase with the energy of extension; without increasing the extension, the oscillation must not increase in amplitude, as this is a function of extension. Instead, the oscillation must increase in energy by increasing in frequency.

The resonant frequency in the modified design was higher for both materials than in the initial design. This is likely due to the increase in cross-sectional area. Each new element placed orthogonally to the direction of the force $\mathbf{F}(s)$ acts as an additional parallel spring, increasing the total stiffness of each cross-sectional cut.

The increase in resonant frequency between materials is therefore explained by the higher Young's modulus of CFRP, in spite of the effect of the greater off-diagonal couplings in the stiffness matrix as a result of the woven nature of a CFRP laminate. Since fibres cross over like ropes between disparate nodes, they are more interconnected.

Since the trace is equal to the sum of eigenvalues $tr(K) = \sum \lambda$ and the same is true for the sum of squares $\mathrm{tr}(K^2) = \sum \lambda^2$, we can confirm that

$$\mathrm{Var}(\lambda) = \frac{\mathrm{tr}(K^2)}{N} - \frac{\mathrm{tr}(K)^2}{N^2} : \mathrm{tr}(K^2) = \sum_i K_{ii}^2 + 2\sum_{i<j} K_{ij}$$

where N is the number of nodes, which means that lowering the off-diagonal elements of the stiffness matrix K_{ij} will reduce the spread of eigenvalues with a sensitivity of $\frac{2}{N^2}$, lowering the higher resonant frequencies but increasing the lower resonant frequencies, especially the fundamental frequency.

4.4 Comparison

The fundamental frequency increased by 36% for Aluminium and 44% for CFRP as a result of the design modifications, with the sacrifice of $\sim$ 100g of additional mass, although the initial design already exceeded the design requirement of $\geq$ 50Hz fundamental frequency. The weight remained reasonable at $<$ 600g.

The stress distribution was initially poor, resulting in a material life of 0 cycles, but was significantly improved in the modified design, to still quite a poor material life of $\sim 18,000$ cycles for aluminium and $\sim$ 900 for CFRP. In any case, despite substantial improvements, the material life target of $1,000,000$ cycles was clearly failed.

Performance metrics aside, it would be difficult to store the needed elastic energy in each step for a smooth running experience.

5 Conclusion

The problem was of increasing the fundamental frequency of an RSP in order that no resonance would occur upon collision with the ground, as this would transfer shock to the leg and hurt the user as well as the material life of the blade. Additional considerations included the increase of material life and the retention of a reasonable blade weight.

A 2-layered approach was taken to FEA in order to develop lo-fi models and inform the design before assessing it with 3D commercial FEA. The approach resulted in multiple new features such as fillet wings, wider fillet radii and support struts which were validated separately.

This study was limited by computational resources for which maximum stress had not converged, implying a significant discretisation error, and a poor initial design to conduct comparisons for fatigue. However, it is clear that fundamental frequency and material life were improved. The modified design is more durable and less prone to resonance while running, although it may lack in its ability to spring the user forward.

A Derivation of N and Q

A curved arc beam is fixed at one end at $s = L$ and a normal load of N and a tangential load of Q is applied to the other end at $s = 0$. Consider a plane swept along the path of the curved beam: the beam elements are cuboids of cross-sectional area A and depth $\mathrm{d}s$. The forces acting on the first element are the load acting on the surface of the element and the reaction forces to prevent acceleration,

$$\mathbf{F} = \begin{bmatrix} Q(0) \\ N(0) \end{bmatrix}, \mathbf{q} = \begin{bmatrix} q_t(0) \\ q_n(0) \end{bmatrix} : \mathrm{d}\mathbf{F} + \mathbf{q}\mathrm{d}s = 0$$

and the boundary reaction force $-\mathbf{q}(\mathbf{0})$ equals the boundary load $\mathbf{F}(0)$. The next element along will experience a load $\mathbf{F}(\mathrm{d}s)$ which is at a slight angle $\mathrm{d}\theta$ to the previous element, such that $\mathbf{F}(d\mathbf{s}) = R(\mathrm{d}\theta)\mathbf{F}(0)$, where $R(\theta)$ is the 2D rotation matrix

$$R(\theta) = \begin{bmatrix} \cos\theta & -\sin\theta \\ \sin\theta & \cos\theta \end{bmatrix}$$

So if $\mathbf{F}(0) = \mathbf{F}$, then $\mathbf{F}(s) = R(\theta)\mathbf{F}$ and the derivatives of constants

$$\mathbf{F}' + \mathbf{q} = 0 = R'(\theta)\mathbf{F}(s) + R(\theta)\begin{bmatrix} N'(s) \\ Q'(s) \end{bmatrix} + R(\theta)\mathbf{q}(s)$$

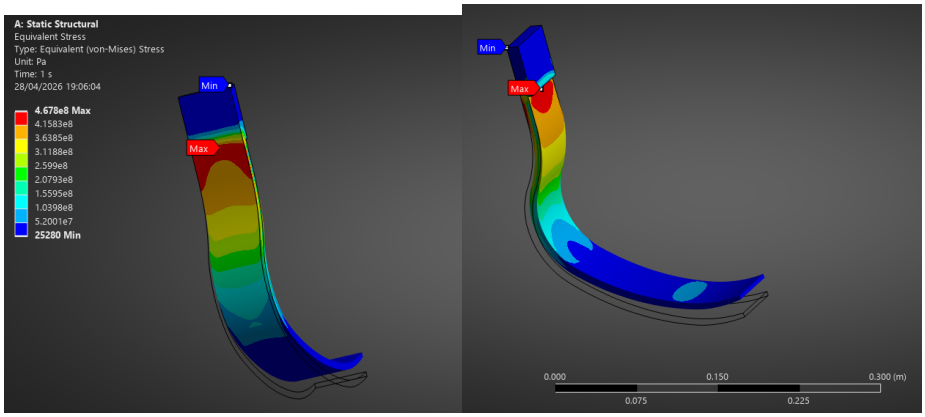
therefore

$$\theta' \begin{bmatrix} 0 & -1 \\ 1 & 0 \end{bmatrix} R(\theta) \begin{bmatrix} N \\ Q \end{bmatrix} + R(\theta) \begin{bmatrix} N' \\ Q' \end{bmatrix} + R(\theta)\mathbf{q}(s) = 0$$

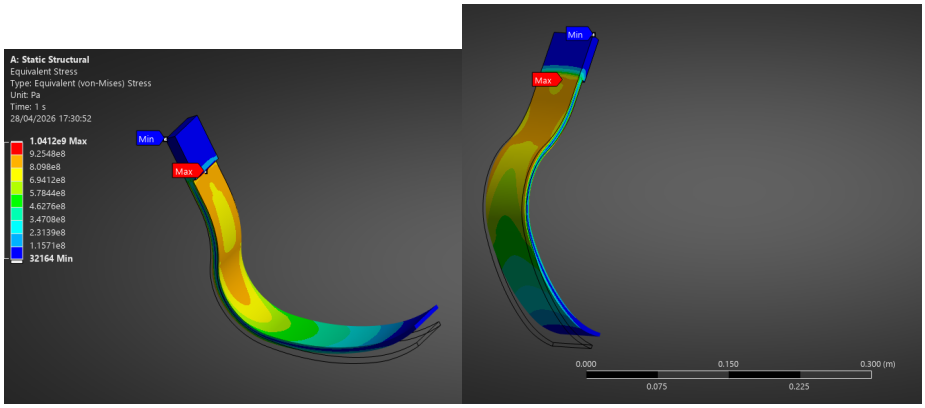
$$N' - \theta' Q + q_t = 0, \quad Q' + \theta' N + q_n = 0$$

which by substituting the complementary equation
$N'' - \theta' N' = 0$ of the derivative $N'' - \theta' Q' = -q_t'$ can be reduced to
$N'' + q_t' + \theta'^2 N + \theta' q_n = 0$ if you assume small deflections (that the curvature θ' is constant).

B Stress Heat Maps

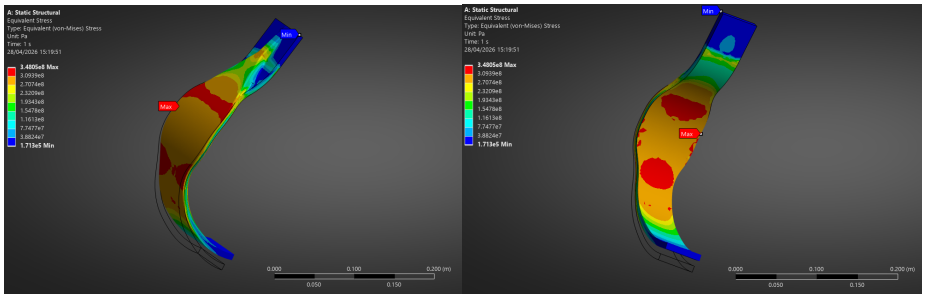


(a) Aluminium

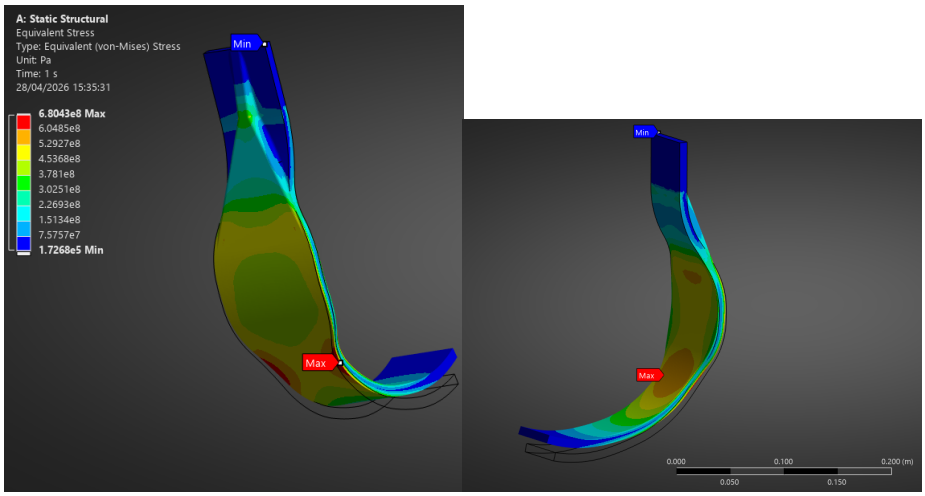


(c) CFRP

Figure 13: Von Mises equivalent stress heat map of initial design.



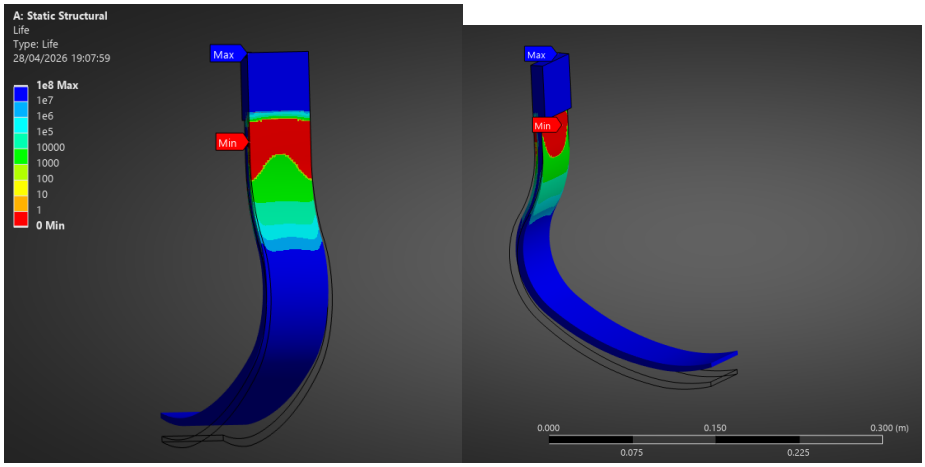
(a) Aluminium



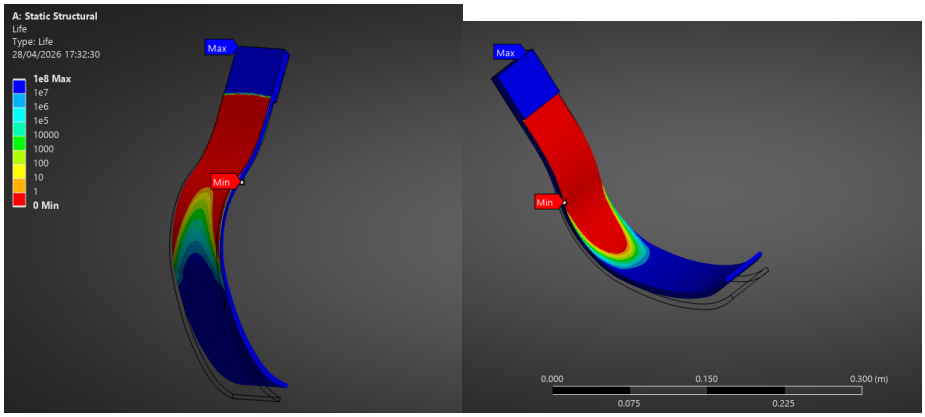
(c) CFRP

Figure 14: Von Mises equivalent stress heat map of modified design.

C Life Heat Maps

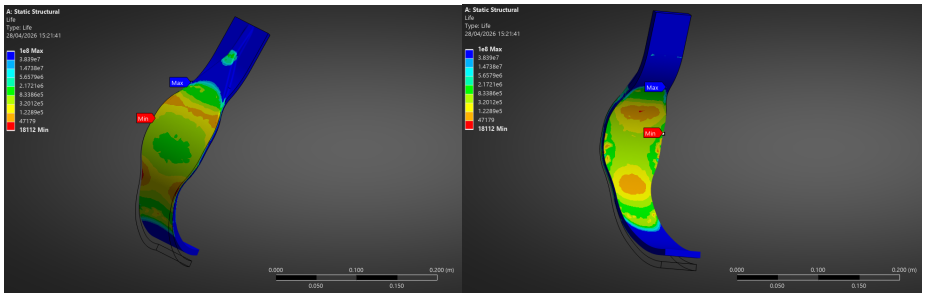


(a) Aluminium

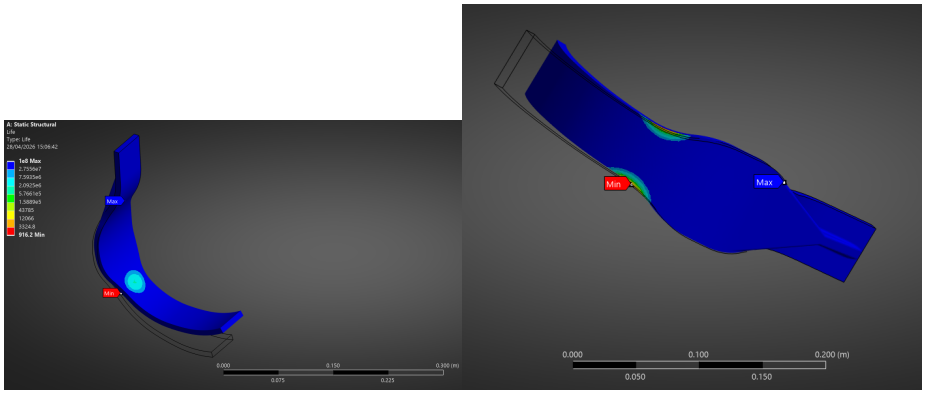


(c) CFRP

Figure 15: Material life heat map of initial design.



(a) Aluminium



(c) CFRP

Figure 16: Material life heat map of modified design.

References

[1] Saleel Hussein Abood and Majid Habeeb Faidh-Allah. "Analysis of Prosthetic Running Blade of Limb Using Different Composite Materials". In: *Journal of Engineering* 25 (Dec. 2019), pp. 15–25. DOI: 10.31026/j.eng.2019.12.02.

[2] The author acknowledges the use of GitHub Copilot to generate frontend code used for preliminary 2D beam simulators. The author confirms that no content generated by AI has been presented as their own work.

[3] IAAF. *IAAF Track Synthetic Surface Testing Specifications IAAF Certification System Track Synthetic Surface Testing Specifications*. Mar. 2011. URL: https://www.worldathletics.org/download/download?filename=87f90dcb-2791-4612-b5fe-2f982aa51199.pdf&urlslug=CERTIFICATION%20PROCEDURES%20-%20IAAF%20Track%20Synthetic%20Surface%20Testing%20Specifications%20(MAR%202011) (visited on 04/29/2026).

[4] S MICHEL, R KIESELBACH, and H MARTENS. "Fatigue strength of carbon fibre composites up to the gigacycle regime (gigacycle-composites)". In: *International Journal of Fatigue* 28 (Mar. 2006), pp. 261–270. DOI: 10.1016/j.ijfatigue.2005.05.005.

[5] Gabriel Leonard Mitu. "Methods and Techniques for bio-systems Materials Behavior Analysis". PhD thesis. Feb. 2014. URL: https://doi.org/10.4995/Thesis/10251/35445.

[6] Essam B. Moustafa and Khalid H. Almitani. "Detecting Damage in Carbon Fibre Composites using Numerical Analysis and Vibration Measurements". In: *Latin American Journal of Solids and Structures* 18 (2021). DOI: 10.1590/1679-78256294.

[7] Robinson. "Determination of ideal body weight for drug dosage calculations". In: *American journal of hospital pharmacy* 40 (2026). URL: https://pubmed.ncbi.nlm.nih.gov/6869387/ (visited on 04/26/2026).